Supplementary Information (SI) for Journal of Materials Chemistry A.


## Supplementary information

### Electrochemically activated copper-based catalyst from coordination polymer for stable hydrogen evolution reaction

Taehun Im,[a,e] Joo-Won Lee,[a,b] Sung-Chul Kim,[c] Sungju Jun,[a,e] Jae-Seung Lee,[e] Min-Seok Kim,[b] Jae Kyun Lee[d] and Sohee Jeong*[a]

[a]Materials Architecturing Research Center, Korea Institute of Science and Technology, 5, Hwarang-ro 14 gil, Seongbuk-gu, Seoul, 02792, Republic of Korea.

E-mail: soheejeong@kist.re.kr

[b]Extreme Materials Research Center, Korea Institute of Science and Technology, 5, Hwarang-ro 14 gil, Seongbuk-gu, Seoul, 02792, Republic of Korea

[c]Advanced Analysis and Data Center, Korea Institute of Science and Technology, 5, Hwarang-ro 14 gil, Seongbuk-gu, Seoul, 02792, Republic of Korea

[d]Brain Science Institute, Korea Institute of Science and Technology, 5, Hwarang-ro 14 gil, Seongbuk-gu, Seoul, 02792, Republic of Korea

[e]Department of Materials Science and Engineering, Korea University, 145, Anam-ro, Seongbuk-gu, Seoul, 02841, Republic of Korea

## Supplementary Figures

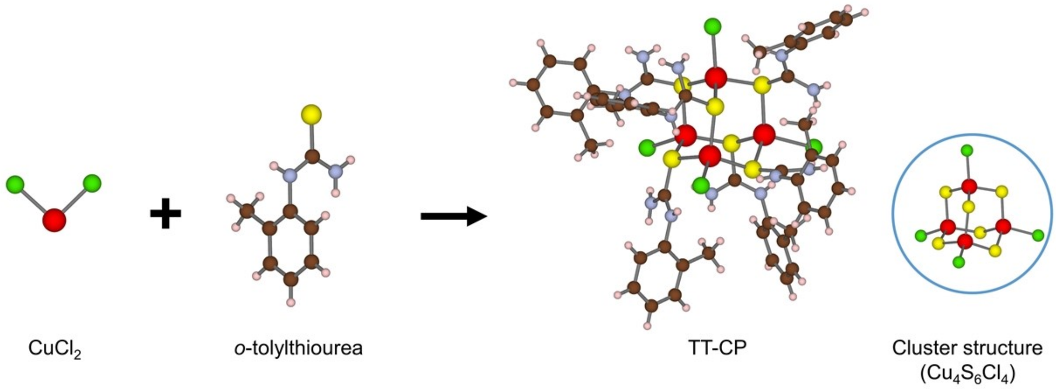


**Fig. S1** Schematic illustration showing the fabrication process of TT-CP by mixing $CuCl_2$ and *o*-tolylthiourea.

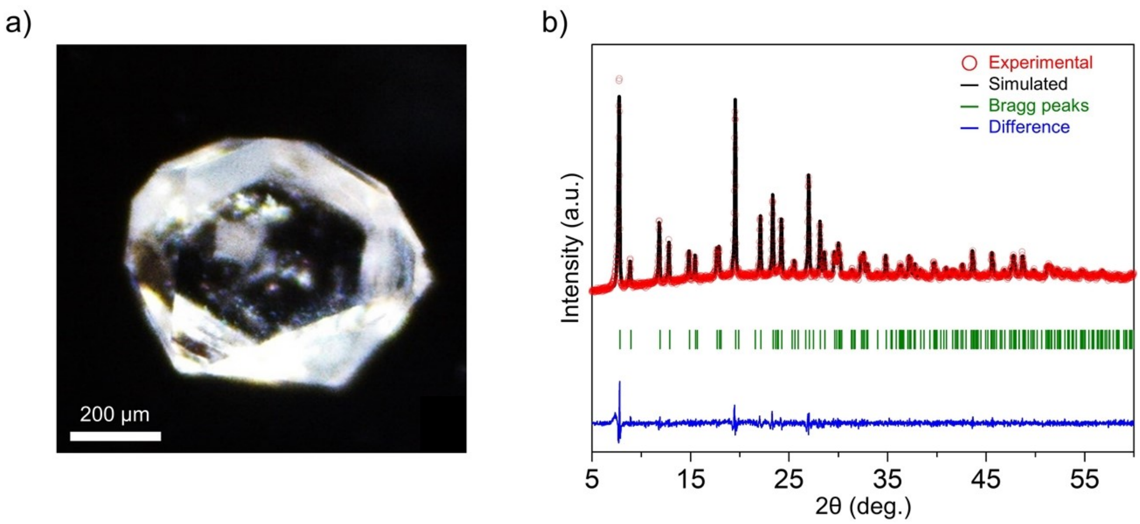


**Fig. S2** (a) Optical microscope image of a TT-CP single crystal. (b) Rietveld refinement result of micrometer-scale TT-CP powders.

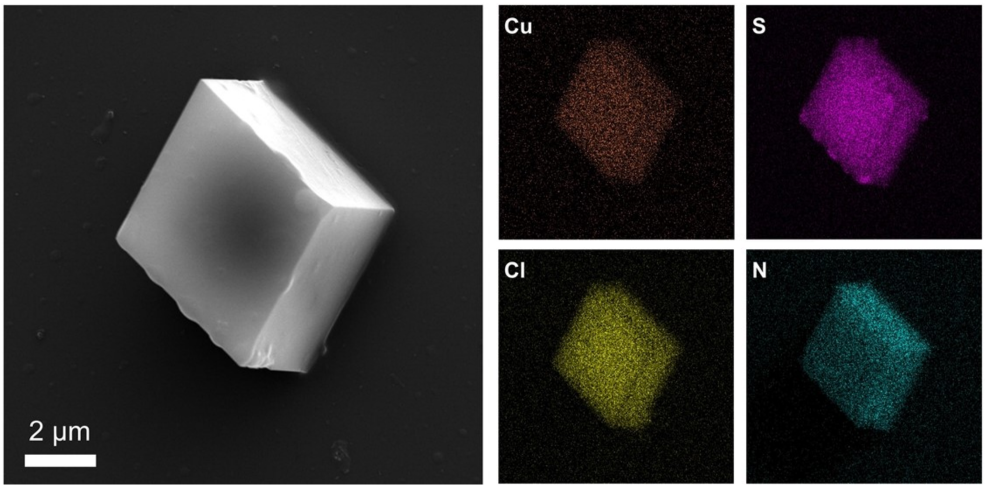


**Fig. S3** SEM image and EDS mapping result of a single TT-CP micrometer-scale powder, where the Cu, S, Cl, C, and S elements are detected.

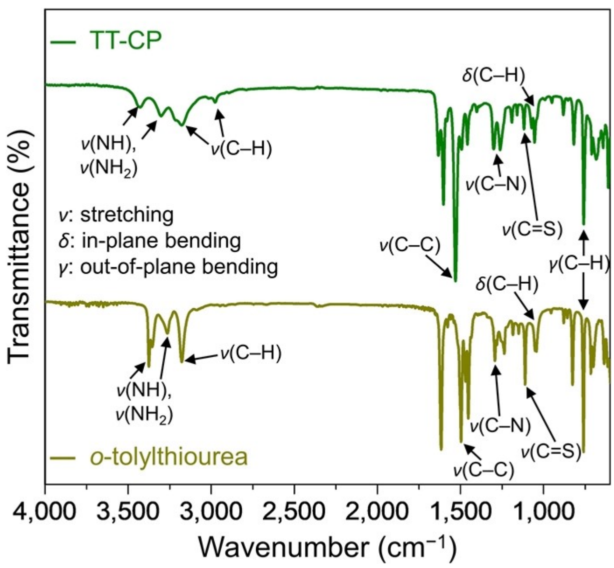


**Fig. S4** FT-IR spectra of *o*-tolylthiourea and TT-CP.

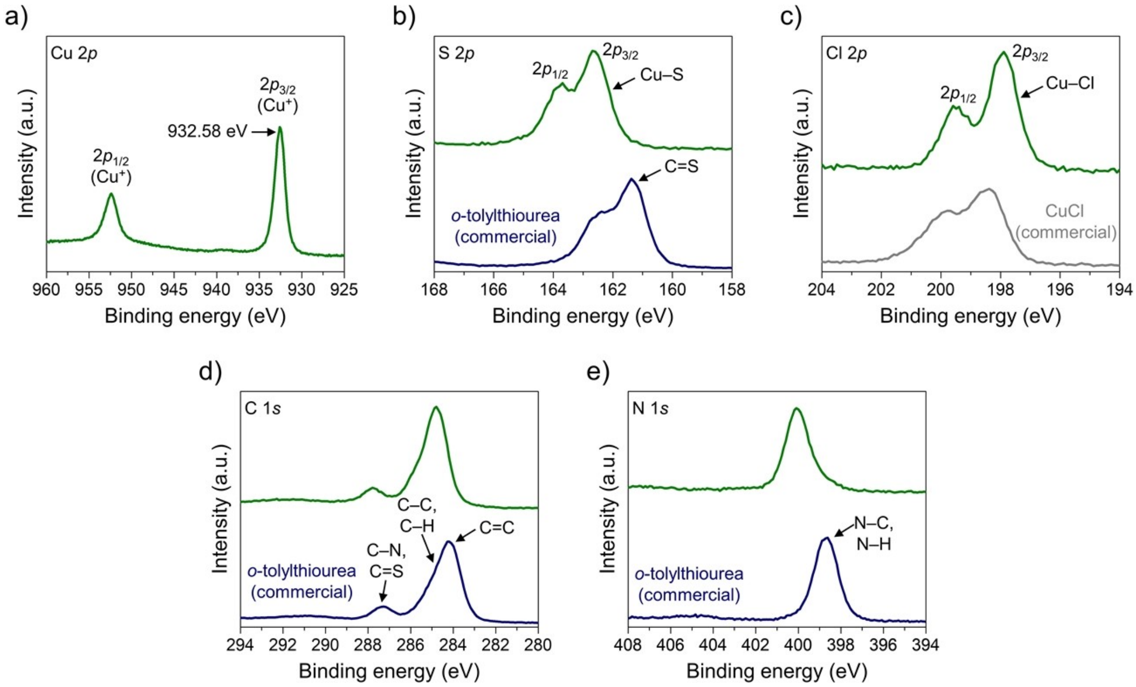


**Fig. S5** XPS spectra of TT-CP measured at the core level region of (a) Cu 2*p*, (b) S 2*p*, (c) Cl 2*p*, (d) C 1*s*, and (e) N 1*s*.

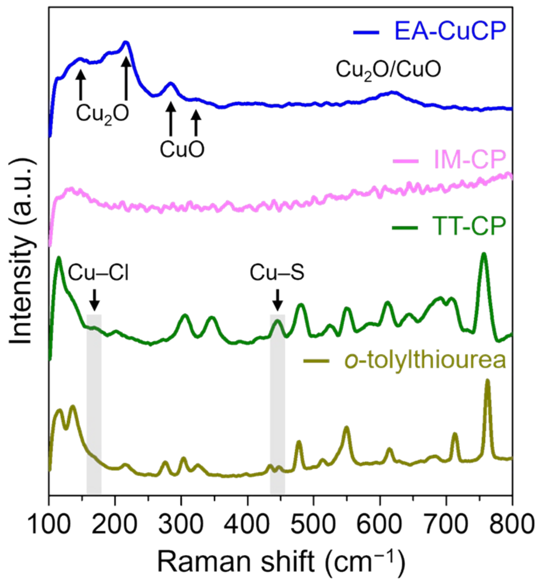


**Fig. S6** Raman spectra of *o*-tolylthiourea, TT-CP, IM-Cu, and EA-CuCP.

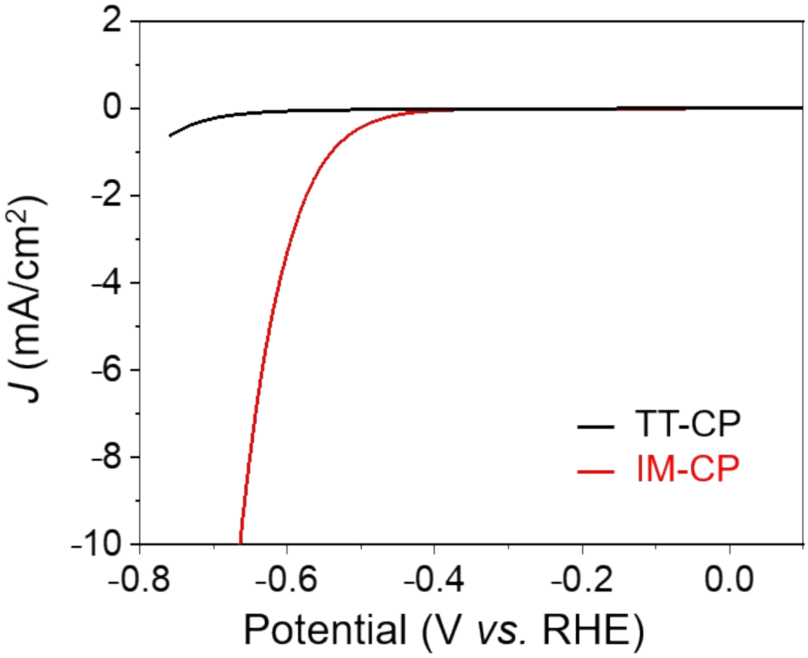


**Fig. S7** HER polarization curves of TT-CP and IM-CP

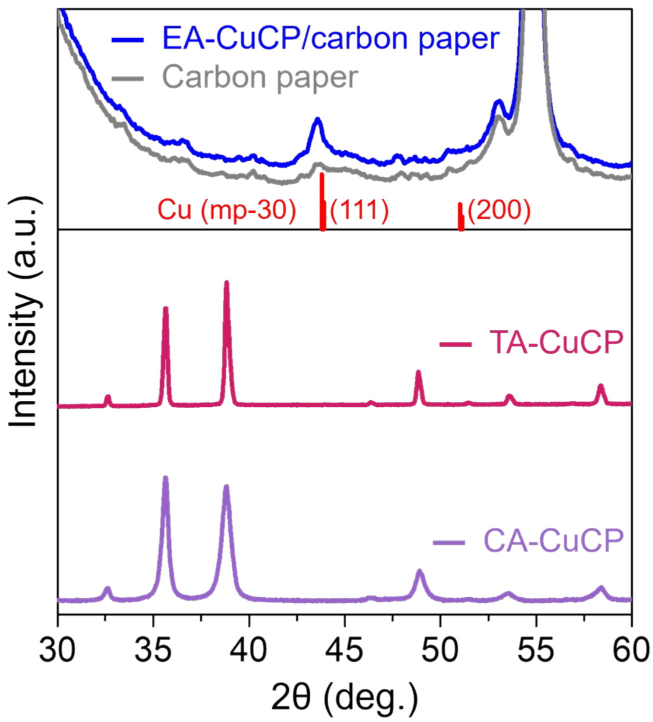


**Fig. S8** PXRD patterns of CA-CuCP, TA-CuCP, and EA-CuCP/carbon paper. Inset red vertical lines present reference diffraction patterns of Cu (mp-30), as obtained from the Materials Project.

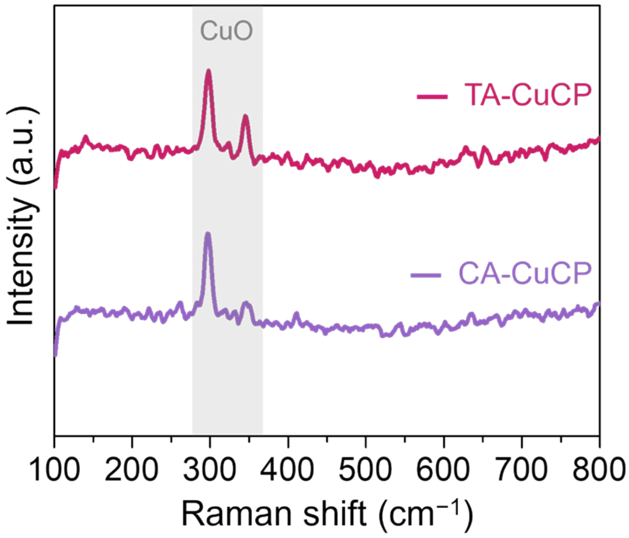


**Fig. S9** Raman spectra of CA-CuCP and TA-CuCP.

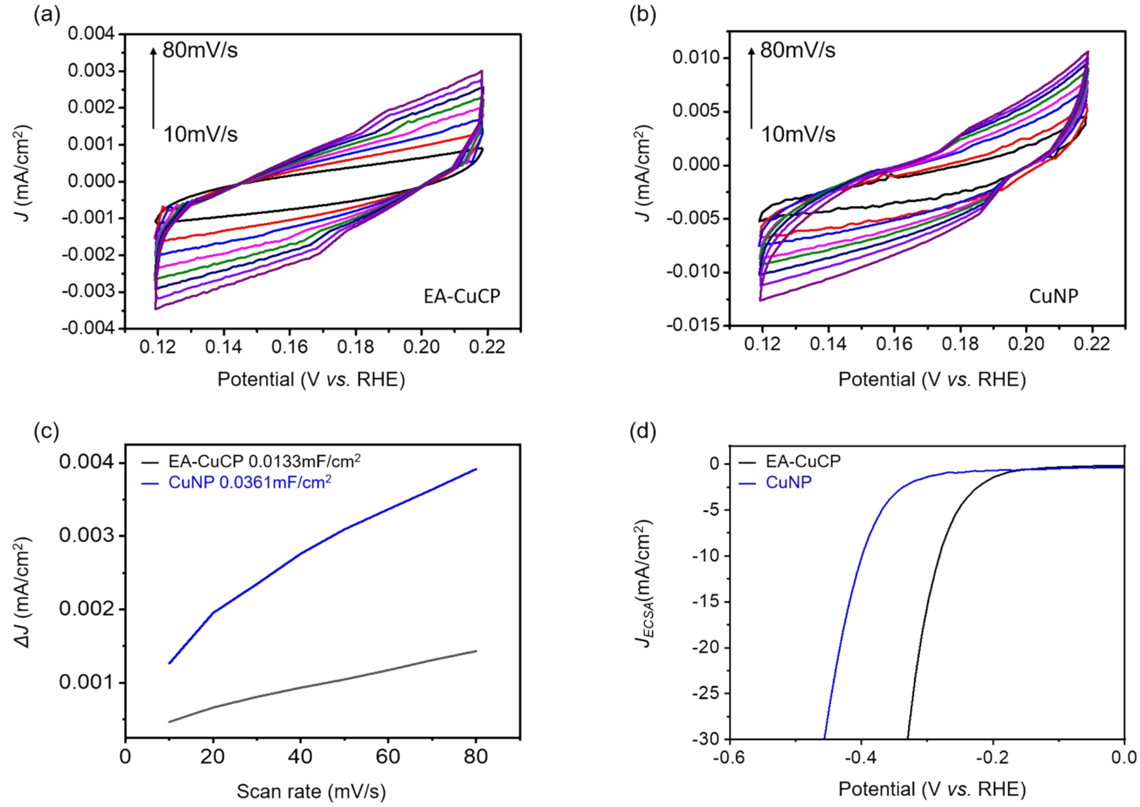


(e)

| | EA-CuCP | CuNP |
|---|---|---|
| ECSA ($cm^2$) | 0.0235 | 0.0638 |

**Fig. S10** Cyclic voltammograms (CV) of Cu catalyst at various scan rates in a 0.5 M $H_2SO_4$ solution: (a) EA-CuCP, (b) CuNP, (c) Average current density ($\Delta j = (j_a - j_c)/2$) against the scan rate showing the double-layer capacitance ($C_{dl}$) extracted from the corresponding CVs. (d) LSV based on the ECSA-specific current density in a 0.5 M $H_2SO_4$ solution. (e) The ECSA obtained by $C_{dl}$ measurement was as follows for each catalyst.

The double layer capacitance ($C_{dl}$) was determined from a CV using the equation: $C_{dl} = \Delta j$ $(j_a - j_c)/2\nu$, where $j_a$ and $j_c$ are anodic and cathodic current densities at $\Delta E = 0.1$ V and $\nu$ is the scan rate in mV/s . The non-Faradic current density based electrochemically active surface area (ECSA) was estimated according to the equation: ECSA = $C_{dl}/C_s$ , (where $C_s$ denoted specific capacitance and was 20-60 μF $cm^{-2}$ in 0.5 M $H_2SO_4$). In this study the value is selected as 40 μF $cm^{-2}$.[1] For the measurement, an electrode with a circle-shaped glassy carbon of 0.3 cm in diameter was used at the end of the rod.

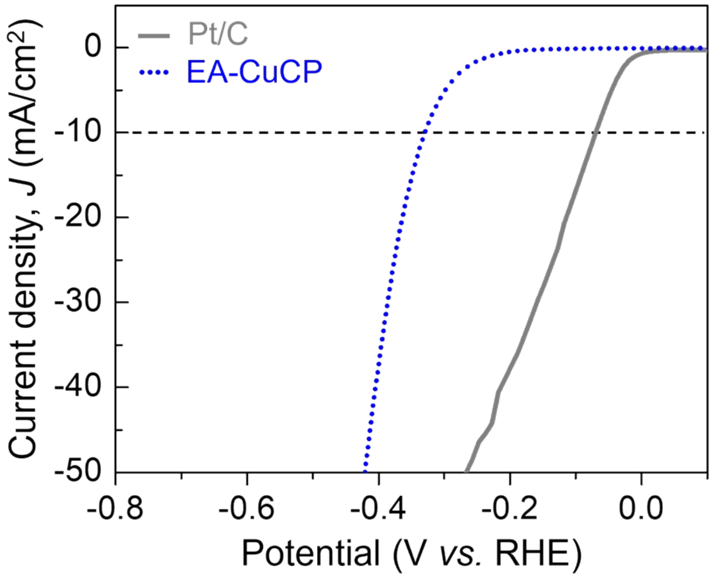


**Fig. S11** HER polarization curves of Pt/C and EA-CuCP.

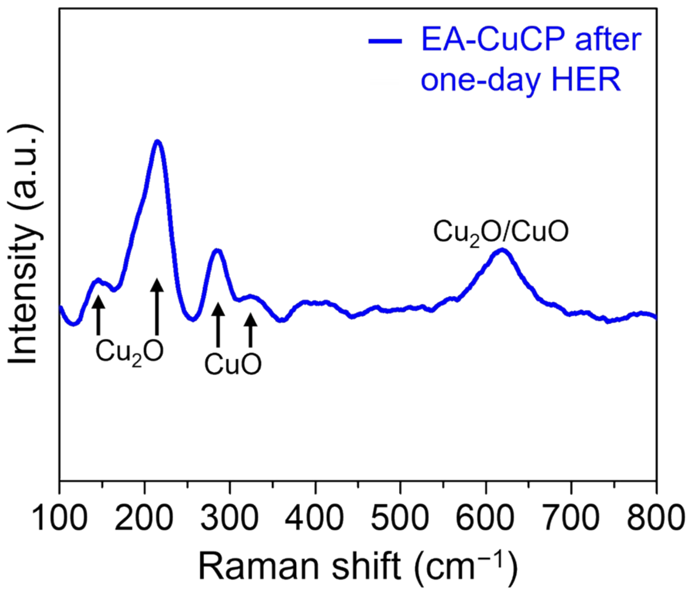


**Fig. S12** Raman spectrum of EA-CuCP after the one-day HER stability test.

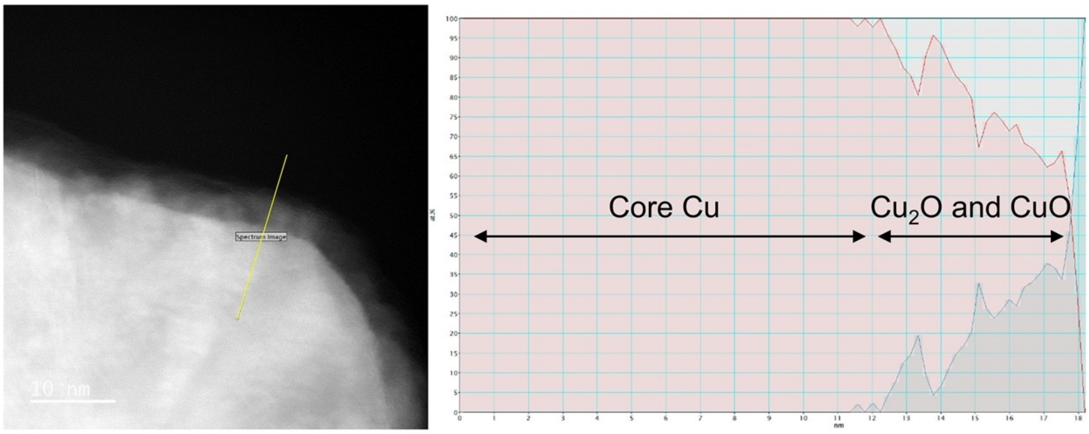


**Fig. S13** EDS line profile measured across the boundary of core Cu and surface oxides ($Cu_2O$ and CuO).

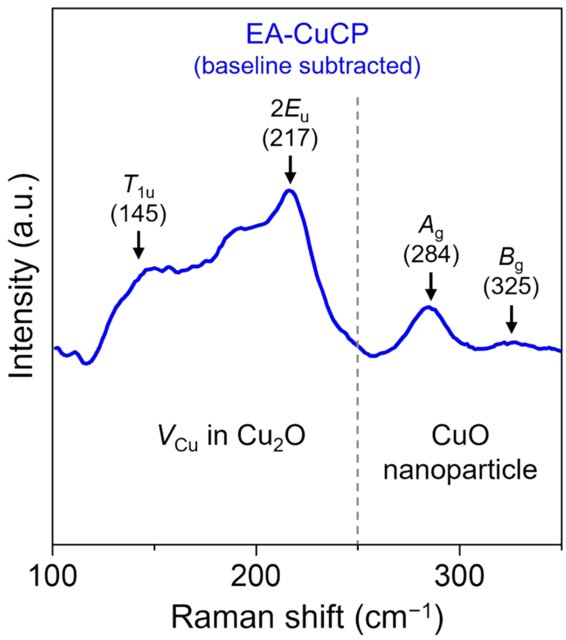


**Fig. S14** Magnified and baseline-subtracted Raman spectrum of EA-CuCP.

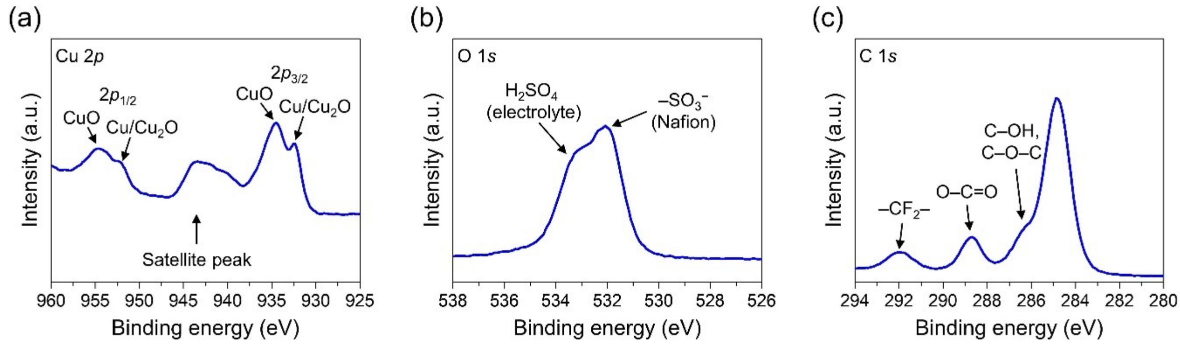


**Fig. S15** XPS spectra of EA-CuCP measured at the core level region of (a) Cu 2*p*, (b) O 1*s*, and (c) C 1*s*.

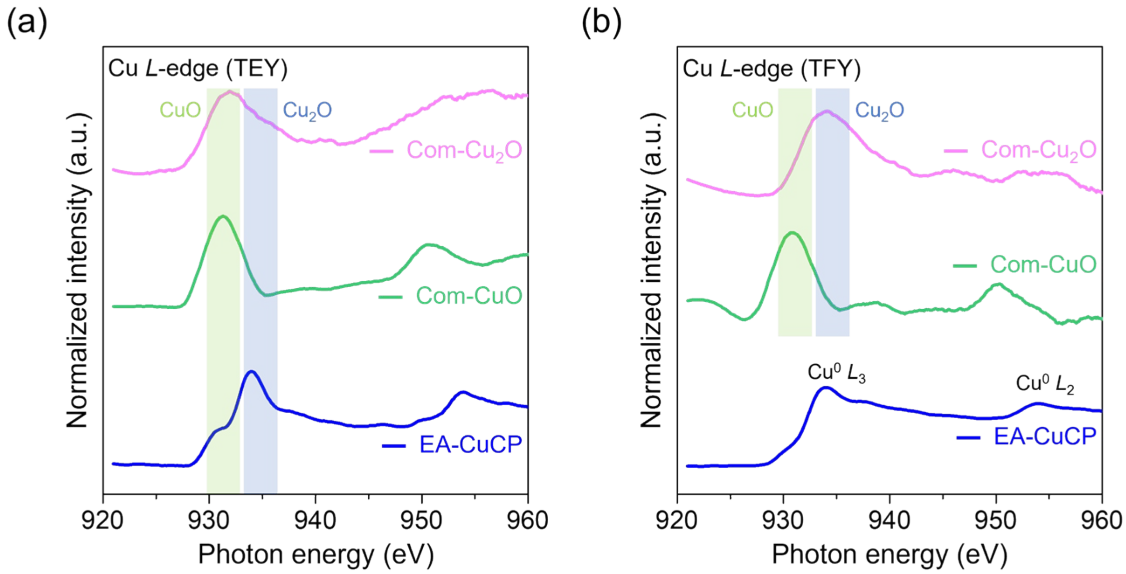


**Fig. S16** Cu *L*-edge NEXAFS spectra of Com-$Cu_2O$, Com-CuO and EA-CuCP recorded by (a) TEY and (b) TFY detection modes.

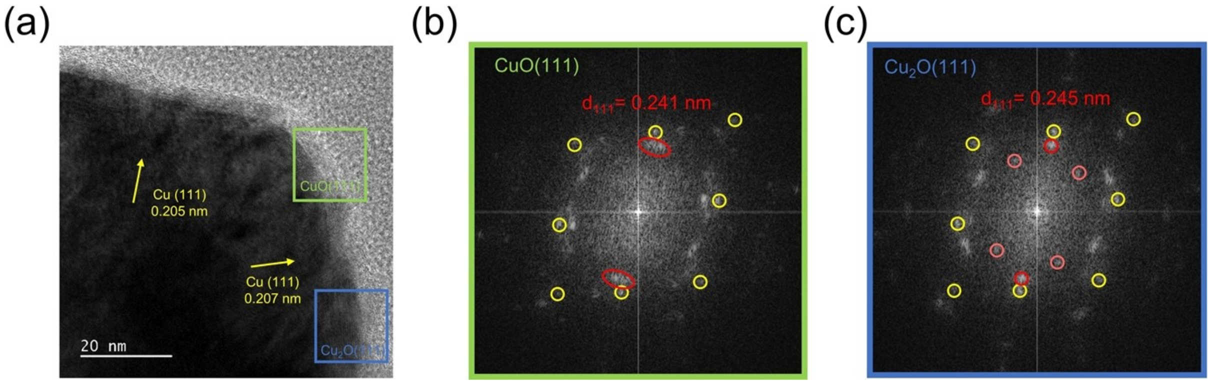


**Fig. S17** (a) HR-TEM image of EA-CuCP. FFT patterns obtained at (b) CuO-rich region and (c) $Cu_2O$-rich region.

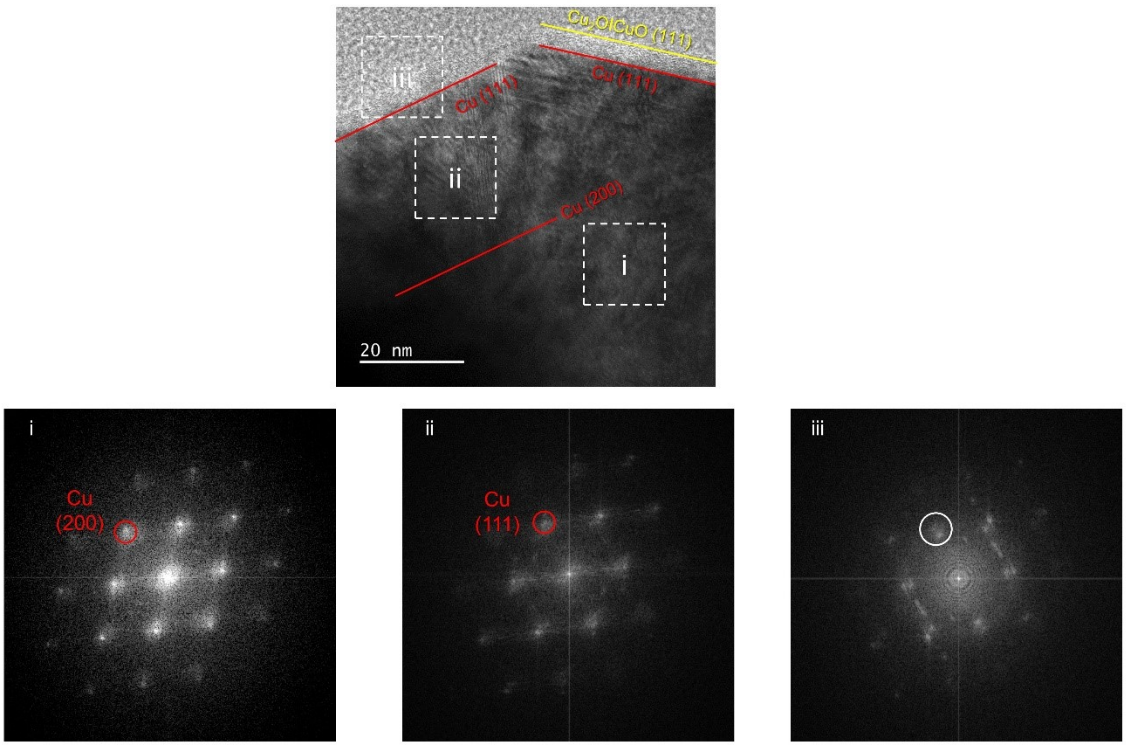


**Fig. S18** HR-TEM image and FFT patterns of EA-CuCP measured at three different regions.

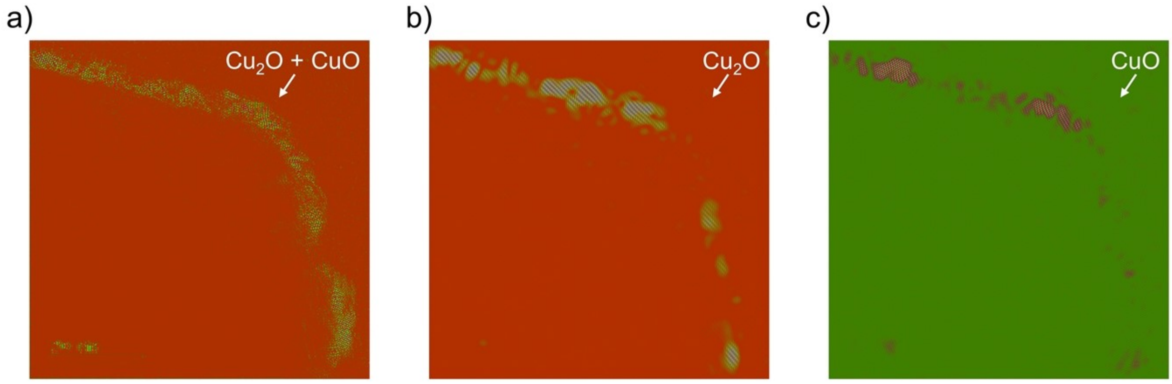


**Fig. S19** Inverse FFT patterns of EA-CuCP with lattice fringes of (a) both $Cu_2O$ and CuO, (b) $Cu_2O$, and (c) CuO highlighted.

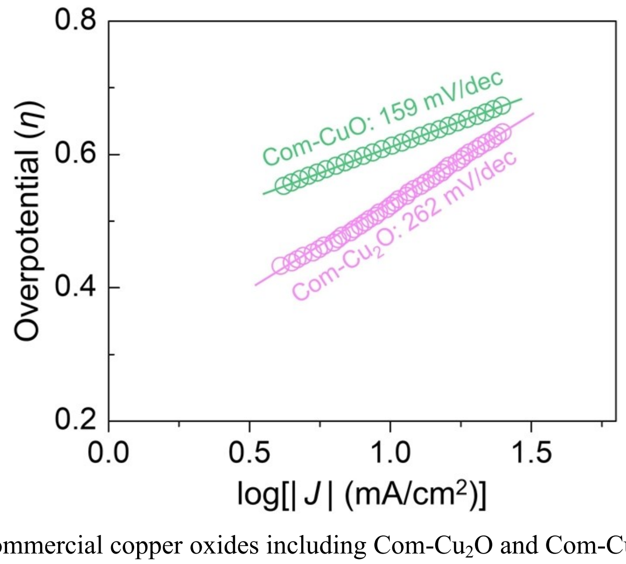


**Fig. S20** Tafel slopes of commercial copper oxides including Com-$Cu_2O$ and Com-CuO.

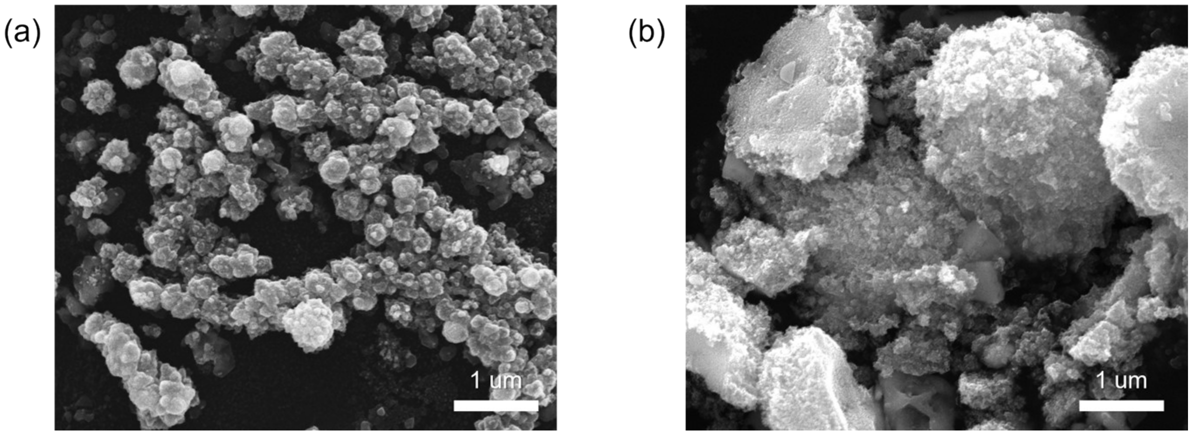


**Figure S21**. SEM images of EA-CuCP (a) before and (b) after (under -20 mA/cm$^2$, 2800 h) the stability test.

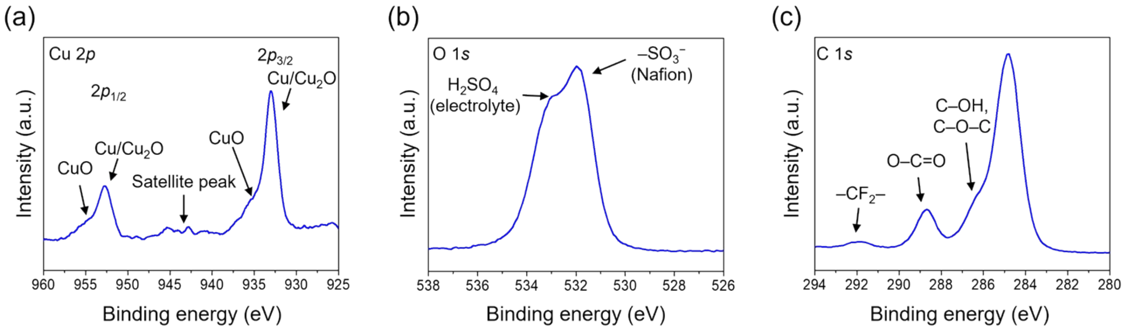


**Figure S22.** XPS spectra of EA-CuCP after stability test (under -20 mA/cm$^2$, 2800 h). (a) Cu 2p, (b) O 1s, and (c) C 1s.

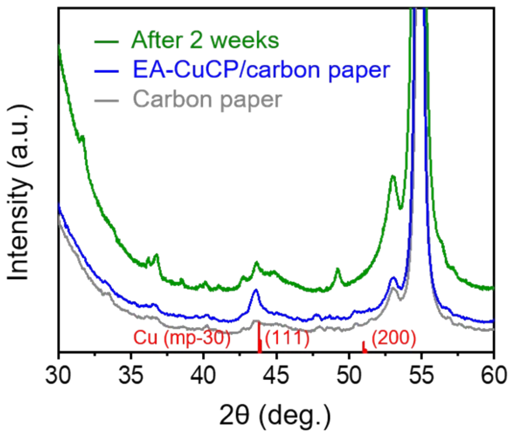


**Figure S23.** XRD pattern of EA-CuCP after stability test (under -20 mA/cm$^2$, 2 weeks).

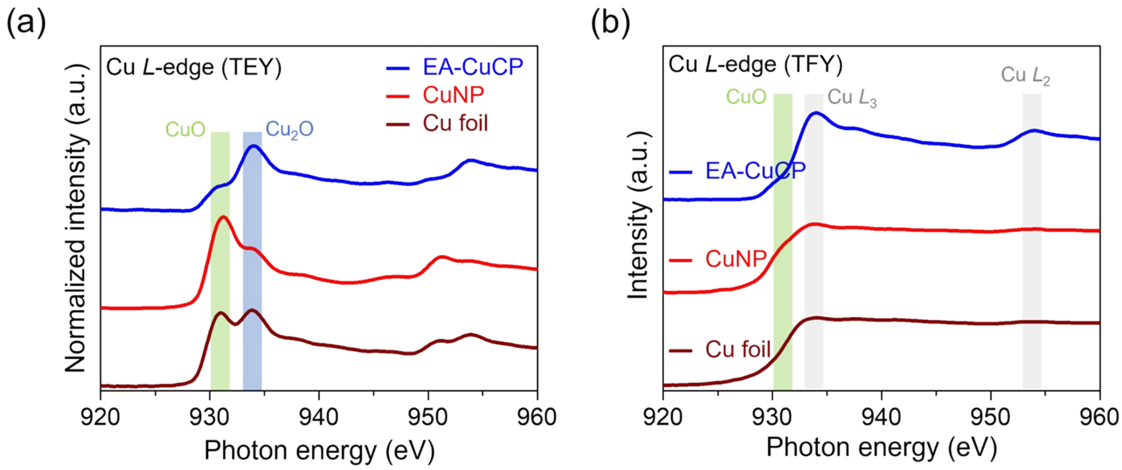


**Fig. S24** Cu *L*-edge NEXAFS spectra of Cu foil, CuNP, and EA-CuCP recorded using the TFY detection mode.

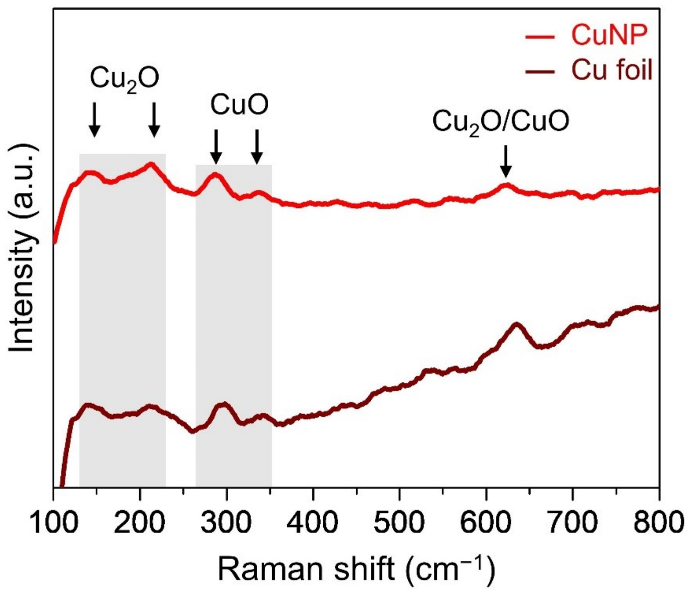


**Fig. S25** Raman spectra of Cu foil and CuNP.

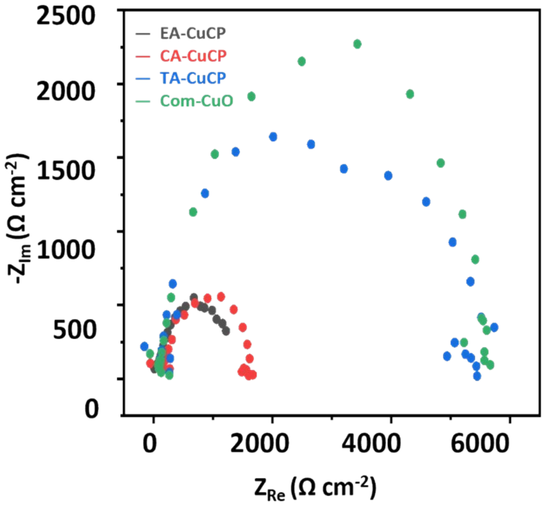


**Fig. S26** Electrochemical impedance spectroscopy analysis of copper-based materials.

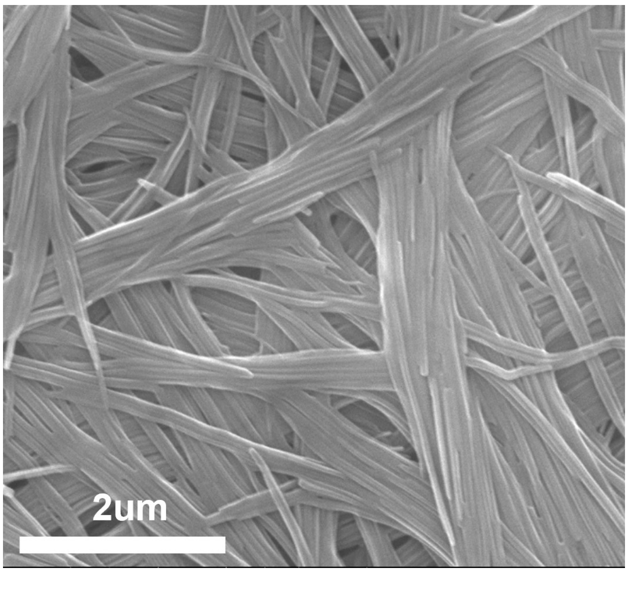


**Fig. S27** SEM image of a TT-CP-mod (Cu:S=1:1)

## Supplementary Tables

| Sample | Space group | Lattice parameters | $R_{exp}$ (%) | $R_{wp}$(%) | $R_p$ (%) | Goodness of fitting |
|---|---|---|---|---|---|---|
| TT-CP | R-3 | a (Å) 19.7045<br>c (Å) 31.6978 | 6.28 | 8.66 | 6.73 | 1.38 |

**Table S1** Fitting parameters for the Rietveld refinement of TT-CP.

**Table S2** Elemental composition of as-synthesized TT-CP.

| Element | Composition (at%) |
|---|---|
| C | 61.76 |
| Cl | 4.67 |
| Cu | 6.02 |
| N | 17.56 |
| O | 1.61 |
| S | 8.38 |

**Table S3** HER performance of previously reported copper-based catalysts.

| | HER overpotential | Stability | Electrolyte | Reference |
|---|---|---|---|---|
| Cu-$Cu_2$ONP@C | 672 mV@−10 mA $cm^{-2}$ | - | 0.4 M $H_2SO_4$ | [1] |
| Pure $Cu_2O$ | 549 mV@−10 mA $cm^{-2}$ | - | 0.5 M $H_2SO_4$ | [2] |
| $Cu_2O$@rGO | 458 mV@−10 mA $cm^{-2}$ | - | 0.5 M $H_2SO_4$ | [2] |
| Cu-$Cu_2O$@C2 | 637 mV@−10 mA $cm^{-2}$ | - | 0.4 M $H_2SO_4$ | [3] |
| $Cu_2O$-200/GCE | 184 mV@−10 mA $cm^{-2}$ | 1000 cycles/ 20 h @ −0.57 V | 1.0 M KOH | [4] |
| Cu mesh | 622 mV@−10 mA $cm^{-2}$ | - | 0.5 M $H_2SO_4$ | [5] |
| $Cu_xO$@Cu M400 | 460 mV@−10 mA $cm^{-2}$ | - | 0.5 M $H_2SO_4$ | [5] |
| $Cu_xO$@Cu M300 | 498 mV@−10 mA $cm^{-2}$ | 20 h @ −2.5 mA $cm^{-2}$ | 0.5 M $H_2SO_4$ | [5] |
| Plasma spray Cu | 182 mV@−10 mA $cm^{-2}$ | 30 h @ −0.35 V (100 mA $cm^{-2}$) | 0.5 M $H_2SO_4$ | [6] |
| Cu/$Cu_2$O-CuO/rGO-400 | 105 mV@−10 mA $cm^{-2}$ | 15 h @ −10 mA $cm^{-2}$ | 1.0 M KOH | [7] |
| EA-CuCP | 331 mV@−10 mA $cm^{-2}$ | 2,800 hr @ −20 mA $cm^{-2}$ | 0.5 M $H_2SO_4$ | This work |

## Supplementary References


[1] P. Muthukumar, V. V. Kumar, G. R. K. Reddy, P. S. Kumar and S. P. Anthony, *Catal. Sci. Technol.*, 2018, **8**, 1414–1422.

[2] M. A. Ramirez-Ubillus, A. Wang, S. Zou, K. Y. Chumbimuni-Torres and L. Zhai, *J. Compos. Sci.*, 2023, **7**, 403.

[3] P. Muthukumar, P. S. Kumar and S. P. Anthony, *Mater. Res. Express*, 2018, **6**, 025518.

[4] M. Wang, X. Cheng and Y. Ni, *Dalton Trans.*, 2019, **48**, 823–832.

[5] N. Alhebshi, H. Huang, R. Ghandour, N. K. Alghamdi, O. Alharbi, S. Aljurban, J. H. He and H. Al-Jawhari, *J. Alloys Compd.*, 2020, **848**, 156284.

[6] W.-J. Kang, Y. Feng, Z. Li, W.-Q. Yang, C.-Q. Cheng, Z.-Z. Shi, P.-F. Yin, G.-R. Shen, J. Yang, C.-K. Dong, H. Liu, F.-X. Ye and X.-W. Du, *Adv. Funct. Mater.*, 2022, **32**, 2112367.

[7] L. Ye and Z. H. Wen, *Chem. Commun.*, 2018, **54**, 6388–6391.